Applied Catalysis B: Environmental 136–137 (2013) 317–324

Contents lists available at SciVerse ScienceDirect

Applied Catalysis B: Environmental

journal homepage: www.elsevier.com/locate/apcatb

Complete methanol oxidation in carbon monoxide streams over Pd/CeO_2 catalysts: Correlation between activity and properties

Yongjin Luo, Yihong Xiao, Guohui Cai, Yong Zheng, Kemei Wei*

National Engineering Research Center of Chemical Fertilizer Catalyst, Fuzhou University, 350002 Fuzhou, PR China

ARTICLE INFO

Article history:
Received 9 November 2012
Received in revised form 9 February 2013
Accepted 13 February 2013
Available online 20 February 2013

Keywords:
Pd/CeO_2
Synthetic techniques
CO
Methanol
Defect sites

ABSTRACT

Three different techniques, a hydrothermal process with impregnation, solution-combustion and common precipitation with impregnation, were employed for the synthesis of 1.5 wt% Pd/CeO_2, and the resulting catalysts were denoted as Pd/HY, Pd/COM and Pd/PI, respectively. These catalysts have been investigated in terms of catalytic co-oxidation of CO and methanol and characterized by means of XRD, BET, SEM, STEM-EDS, CO chemisorption, XPS, Raman, O_2-TPD, H_2-TPR and CO-TPD measurements. Activity results show that a rapid catalytic oxidation of CO following the Mars-van Krevelen-type mechanism favors the complete methanol oxidation at low temperature. Consequently, the Pd/HY catalyst with the highest degree of defect sites connected with the mobility of activated oxygen shows the best catalytic performance. And the generation of more defect sites demonstrated by Raman is assumed for the low crystallinity and small crystallite size of CeO_2 synthesized through a hydrothermal process while the high mobility of activated oxygen is evidenced by O_2-TPD and H_2-TPR. Additionally, the outstanding catalytic performance of Pd/HY is also associated with its high Pd dispersion and stable PdO_x species as well as good redox behavior.

1. Introduction

In order to meet more and more stringent pollution regulations and realize a sustainable energy supply, many researchers focus on the alternative fuels of automobiles [1–3]. And methanol has received a lot of attention due to its low cost and abundance, which can be produced from a wide variety of renewable sources [4,5]. Moreover, methanol proves to have the potential to increase engine performance and efficiency because of excellent combustion properties [6,7], e.g., elevated knock resistance, high heat of vaporization, non-sooting, high oxygen content and low carbon/hydrogen ratio.

As a result, compared to gasoline and diesel, the vehicles operating on methanol-fuel emit less conventional pollutants like CO, total hydrocarbons (THC) and NO_x. Despite its advantages, the use of methanol as a fuel has met resistance due to that it can produce significant amounts of partial oxidation emission such as formaldehyde and unburned methanol because of the incomplete combustion of methanol fuel especially during the cold start [8]. At the moment, the oxidation catalysts exhibit poor performance since the temperatures of emission and catalyst bed are very low, resulting in the release of a considerable amount of emission into the air. It is known that the methanol and formaldehyde are hazardous to the environment and human health. Hence, exploring an efficient catalyst for complete methanol oxidation at low temperature is of great importance.

Currently, several studies have been carried out with the aim to get insights into the high performance of complete methanol oxidation in the absence of CO [9–12]. Actually, the existence of CO in methanol-fueled vehicle exhaust will be adsorbed rapidly and strongly on a noble metal catalyst at low temperature, thereby preventing the reaction of methanol [13,14]. In that case, complete methanol oxidation can only be achieved at temperatures that are high enough to remove CO either by desorption or by reaction with oxygen. However, the abatement of methanol needs to be proceeded at low temperature. Thus, the realization of co-oxidation of CO and methanol at low temperature is meaningful and challenging.

Until now, most of the supported catalysts reported for complete methanol oxidation were with γ-Al_2O_3 as a carrier. It was proposed that there is a competitive adsorption on the same active sites between O_2, CO and H_2 for preferential oxidation of CO (PROX) reaction if the support is inert like γ-Al_2O_3 [15]. Such a competitive Langmuir–Hinshelwood reaction mechanism also applies to the simultaneous oxidation of CO and methanol if γ-Al_2O_3 is adopted as a support.

The use of CeO_2 as a support for precious metals has attracted considerable attention because a strong interaction exists between CeO_2 and noble metal [16,17]. And the reactive O will be provided by CeO_2 at the interface of CeO_2 and noble metal or directly the

* Corresponding author. Tel.: +86 591 8373 8808; fax: +86 591 8373 8808.
E-mail address: kemeiwei2010@sina.cn (K. Wei).

0926-3373/$ – see front matter © 2013 Elsevier B.V. All rights reserved.
http://dx.doi.org/10.1016/j.apcatb.2013.02.020

surface lattice oxygen of CeO_2 [15], resulting in a non-competitive adsorption and an enhancement of CO and methanol co-oxidation at low temperature. Therefore, a model catalyst Pd/CeO_2 applied to the co-oxidation of CO and methanol is feasible and worthy of investigation. And synthetic technique is the most important factor that closely linked to the properties of catalysts. In the present work, three types of Pd/CeO_2 catalysts have been prepared via different methods and their catalytic performances in the co-oxidation of CO and methanol were correlated with properties.

2. Experimental

2.1. Catalyst preparation

Three types of Pd/CeO_2 catalysts were synthesized using a hydrothermal process with impregnation, solution-combustion and common precipitation with impregnation methods, respectively. And the corresponding catalysts were denoted as Pd/HY, Pd/COM and Pd/PI. All the obtained catalysts were crushed, and sieved to a size range of 30–80 mesh and the theoretical loading of Pd is 1.5 wt% for CeO_2.

In the hydrothermal process, 10.96 g of $(NH_4)_2Ce(NO_3)_6$ and 3.60 g of urea (urea/Ce molar ratio = 3) were dissolved in 40 mL of distilled water separately. Then these two solutions were mixed together and transferred into a 100 mL Teflon-lined stainless steel autoclave, which was maintained at 180 °C for 12 h and subsequently cooled to room temperature naturally. The precipitate was then collected by centrifugation, washed with distilled water sufficiently and then dried at 110 °C overnight. A cubic-CeO_2 is detected in the obtained sample by X-ray powder diffraction (XRD), and the palladium was deposited by incipient impregnation method with an aqueous $Pd(NO_3)_2$ as metal precursor. During this process, the impregnated sample was kept at room temperature for 12 h, dried at 80 °C for 4 h and calcined in muffle oven at 600 °C for 4 h.

The detailed solution-combustion method [18] was as follows: 9.56 g of $(NH_4)_2Ce(NO_3)_6$ was dissolved in 15 mL of distilled water in a porcelain crucible with 100 mL capacity. And 1.5 mL of $Pd(NO_3)_2$ aqueous solution (the concentration of Pd^{2+} = 30 g/L) and 3.45 g of $C_2H_5NO_2$ were added to the Ce-containing solution. Then the porcelain crucible was introduced into a muffle furnace maintained at 350 °C to yield a solid product by ignition, which was finally calcined at 600 °C for 4 h.

For the precipitation method, the Na_2CO_3 aqueous solution was added dropwise to the aqueous solution of $(NH_4)_2Ce(NO_3)_6$ under stirring until the final pH was kept at 9. The resultant precipitate was centrifuged, extensively washed with distilled water, then dried at 110 °C overnight and calcined at 600 °C for 4 h. The acquired sample was impregnated by palladium in the same manner as described for Pd/HY.

2.2. Catalytic activity measurement

Catalytic combustion reactions were carried out in a fixed-bed continuous-flow reactor packed with 0.1 g of catalyst under atmospheric pressure. The temperature of the catalyst bed was tested as reaction temperature by inserting a thermal couple into the catalyst. Then, the gas mixture containing 2000 vppm CH_3OH, 2000 vppm CO, 1 vol% O_2 and balance He was fed into the reactor with a space velocity of 60,000 mL g^{-1} h^{-1}. The effluent gases passing before and after the catalyst were analyzed by an on-line GC equipped with a TCD for O_2, CO, and CO_2 separation and a FID for the detection of methanol. Catalytic activity was measured in the range of 60–160 °C and the measurement was taken after maintained for 30 min at each testing temperature. Conversion of CO was calculated as follows:

$$\text{CO conversion}\,(\%) = \frac{[CO]_{in} - [CO]_{out}}{[CO]_{in}} \times 100 \quad (1)$$

where $[CO]_{in}$ and $[CO]_{out}$ were the CO concentrations in the feed gas and products, respectively.

The conversion of methanol to CO_2 was calculated as follows:

Methanol conversion to CO_2 (%) =

$$\frac{[CO_2]_{out} - [CO_2]_{2000ppm} \times \text{CO conversion}\,(\%)}{[CO_2]_{2000ppm}} \times 100 \quad (2)$$

where $[CO_2]_{out}$ was the CO_2 concentration in the products and $[CO_2]_{2000ppm}$ corresponded to 2000 vppm of CO_2.

2.3. Characterization of the catalysts

The X-ray powder diffraction (XRD) patterns of samples were recorded on a PANalytical X'Pert Pro diffractometer at 40 kV and 40 mA with a step size of 0.0167°, using Co-K_α radiation and then revised by Cu-K_α. The textural properties were carried out at −196 °C on a TriStar 3000 apparatus using nitrogen adsorption/desorption method. The samples were degassed at 300 °C for more than 3 h under vacuum before the measurements.

The morphologies of samples were observed by scanning electron microscopy (SEM, Hitachi S-4800), which was operated at 5.0 kV. Scanning TEM (STEM)-EDS characterizations were performed with a FEI Technai G2 F20 microscope operating at 200 kV.

Dispersions of Pd in the catalysts were determined by CO chemisorption, which were carried out on an AutoChem 2920 instrument equipped with a TCD. In order to determine the accurate dispersion on CeO_2 supports, which can also adsorb CO, an O_2–CO_2–H_2–CO pulse method [19] was adopted. First, 50 mg of the sample was reduced in a pure H_2 stream at 400 °C for 0.5 h and then purged with pure He for 0.5 h. After cooling down to room temperature, the sample was exposed to O_2 gas at 30 mL/min for 5 min. Second, carbon dioxide was fed to the sample at 30 mL/min for 5 min, followed by purging with He for 5 min. Third, pure H_2 was fed to the sample at 30 mL/min for 5 min, and then the sample was purged with He for 20 min. To the end, 5 vol% CO/He was pulsed until the intensity of the peak was a constant value. Pd dispersion was evaluated from the consumption of CO, assuming a linear CO adsorption on Pd (CO:Pd = 1:1).

The X-ray photoelectron spectroscopy (XPS) measurements were made on a Physical Electronics Quantum 2000 spectrometer. A monochromatic Al-K_α source (K_α = 1486.6 eV) and a charge neutralizer were equipped in the instrument. And the surface charging effect was corrected by setting the binding energy of adventitious carbon (C 1s) at 284.6 eV.

The Raman spectra were acquired on a Renishaw inVia Reflex Raman spectrometer using an excitation laser line of 325 nm, in a range of 200–1000 cm^{-1}. For each spectrum, 20 scans were accumulated in the spectral window, being the samples in powder form.

The temperature-programmed desorption of O_2 (O_2-TPD) was also performed on the AutoChem 2920 instrument. First, 50 mg of the sample was heated in pure O_2 from room temperature to 500 °C and held for 0.5 h, subsequently cooled to room temperature in He atmosphere. Then the sample was heated from room temperature to 800 °C in helium at a heating rate of 10 °C/min.

The temperature-programmed reduction of H_2 (H_2-TPR) was conducted using the same apparatus as for CO chemisorption, and 50 mg of sample was used in each measurement. The samples were first treated in a He stream at 300 °C for 0.5 h. After being cooled down to room temperature in the same atmosphere, the samples were swept with 10 vol% H_2/Ar until the baseline on the recorder

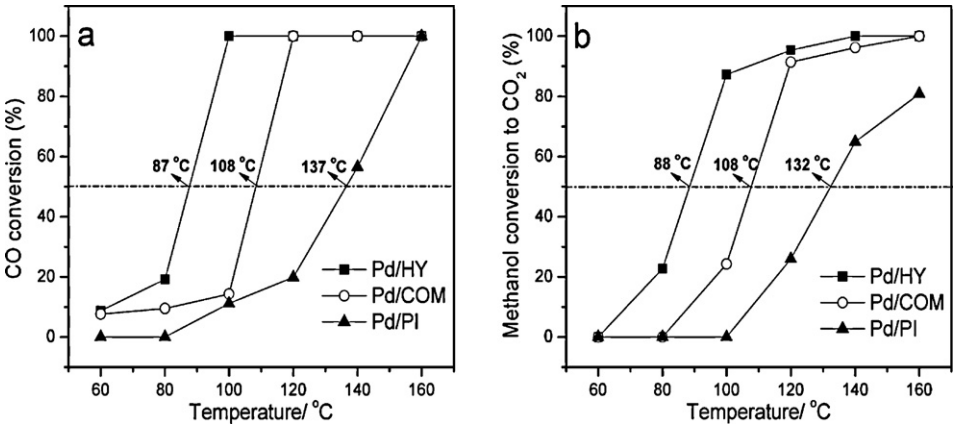

Fig. 1. (a) CO and (b) methanol conversions as function of temperature over Pd/HY, Pd/COM and Pd/PI.

remained unchanged. Then the samples were heated in 10 vol% H_2/Ar from room temperature to 600 °C at a rate of 10 °C/min.

The temperature-programmed desorption (TPD) of CO (CO-TPD) was carried out with a U-type quartz tubular reactor connected to an online mass spectrometer. The sample was first pretreated under He at 500 °C for 0.5 h to remove carbonate and surface chemisorbed oxygen species, and then cooling down to room temperature. After that, CO was chemisorbed on the catalyst by exposing it to a stream of 1 vol% CO/He gas at 30 °C for 1 h. Then, the sample was flushed with He for 30 min, followed by heating to 600 °C at 10 °C/min under the flow of He with a flow rate of 60 mL/min. The signals at mass-to-charge (m/z) ratios of 28 (CO), 32 (O_2) and 44 (CO_2) were monitored on the mass spectrum. And the profile of CO had been deducted from the contribution of m/z = 28 fragment of CO_2.

3. Results and discussion

3.1. Catalytic oxidation

Fig. 1a and b present the catalytic activities of Pd/HY, Pd/COM and Pd/PI catalysts for CO and methanol oxidation, respectively. As expected, it can be seen that the complete conversion of methanol to CO_2 takes place at a higher temperature than that of CO over all catalysts. It is due to a stronger adsorption of CO on the active noble metal [13,14], causing reduced active sites for activating methanol and thus an inhibition of complete methanol oxidation. Hence, in order to obtain a high reactive catalyst for complete methanol oxidation at low temperature, a rapid oxidation of CO is needed.

From Fig. 1a, it can be seen that the Pd/HY catalyst exhibits the highest activity of CO oxidation attaining a lowest light-off temperature (T_{50}), 87 °C. For Pd/COM and Pd/PI, the light-off temperatures increase up to 108 and 137 °C respectively. Meanwhile, as seen in Fig. 1b, the best performance for complete methanol oxidation is also found on Pd/HY while the medium activity exists on Pd/COM. Consequently, the catalytic activities of CO and methanol co-oxidation follow the order of Pd/HY > Pd/COM > Pd/PI.

From the significant differences in catalytic behaviors, it is induced that the catalytic properties are strongly affected by the synthesis technique. It is mentioned above that the achievement of complete methanol oxidation at low temperature needs a rapid reaction of CO oxidation. And it is generally accepted that the CO oxidation over ceria-based catalysts follows Mars-van Krevelen-type mechanism [20], where the release of surface lattice oxygen from CeO_2 is crucial. On the basis, a potential reaction model is demonstrated in Scheme 1. In all, it is concluded that the synthesis technique exerts a basic influence on the mobility of oxygen, which in turn determines the final reactivity of catalysts.

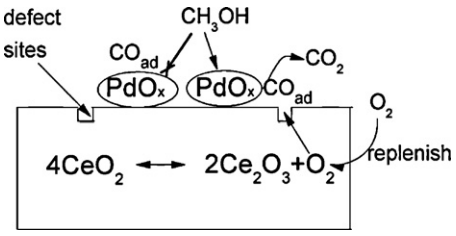

Scheme 1. Reaction model of CO and methanol co-oxidation over Pd/CeO_2 catalysts.

3.2. Characterizations of the catalysts

The phase structures of catalysts were investigated by XRD. As shown in Fig. 2, no diffraction peaks corresponding to PdO or Pd phase and only diffraction peaks due to the cubic CeO_2 phase are observed. A possible reason can be that the palladium species dispersed well on the catalyst surface or incorporated into the CeO_2 lattice to form a solid solution [21]. Additionally, the average crystallite sizes calculated by applying the Debye–Scherrer formula on the CeO_2 (1 1 1) diffraction peaks and lattice parameters of catalysts are listed in Table 1.

From Table 1, it is found that the crystallite size of CeO_2 in Pd/HY is far smaller than that in the other two catalysts. And smaller crystallites may mean the presence of more crystal defects which are

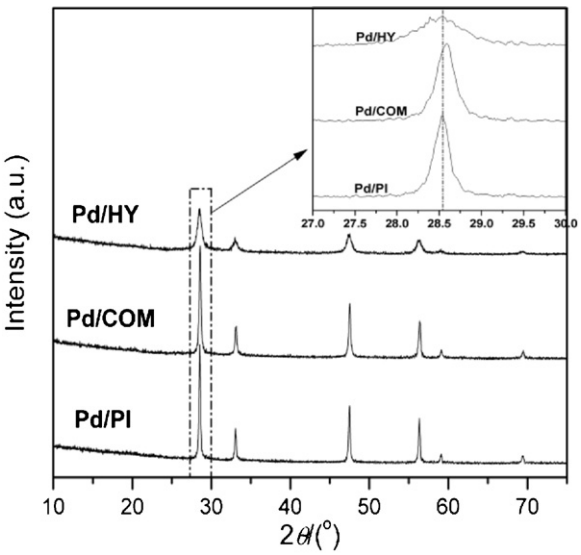

Fig. 2. XRD patterns of Pd/HY, Pd/COM and Pd/PI catalysts.

Table 1
Textural and structural properties of Pd/HY, Pd/COM and Pd/PI catalysts.

Catalyst	Average pore radius (nm)	Pore volume (cm^3/g)	S_{BET} (m^2/g)	Lattice parameters (A)	Crystallite size (nm)
Pd/HY	3.8	0.078	42	5.4184	13.0
Pd/COM	17.6	0.089	8	5.4054	32.3
Pd/PI	–	–	0	5.4133	39.9

Table 2
The content of Ce^{3+} in Ce on the surface, the value of I_{580}/I_{460}, apparent Pd dispersion, average Pd particle size and Pd content of Pd/HY, Pd/COM and Pd/PI catalysts.

Catalyst	Ce^{3+} in Ce[a] (%)	I_{580}/I_{460}[b]	Apparent Pd dispersion[c] (%)	Average Pd particle size[c] (nm)	Pd content[d] (wt%)	
					Total	Surface
Pd/HY	17.2	0.79	22.8	4.9	1.49	0.22
Pd/COM	20.0	0.48	4.5	24.9	1.48	0.65
Pd/PI	14.1	0.43	0	–	1.46	1.35

[a] Deduced from XPS analysis.
[b] Deduced from Raman analysis.
[c] Calculated based on CO chemisorption results.
[d] The Pd content in the catalyst was analyzed using atomic absorption spectrometry (AAS) after being dissolved by HCl and H_2O_2 mixed aqueous; the surface Pd was removed by a nitric-acid treatment.

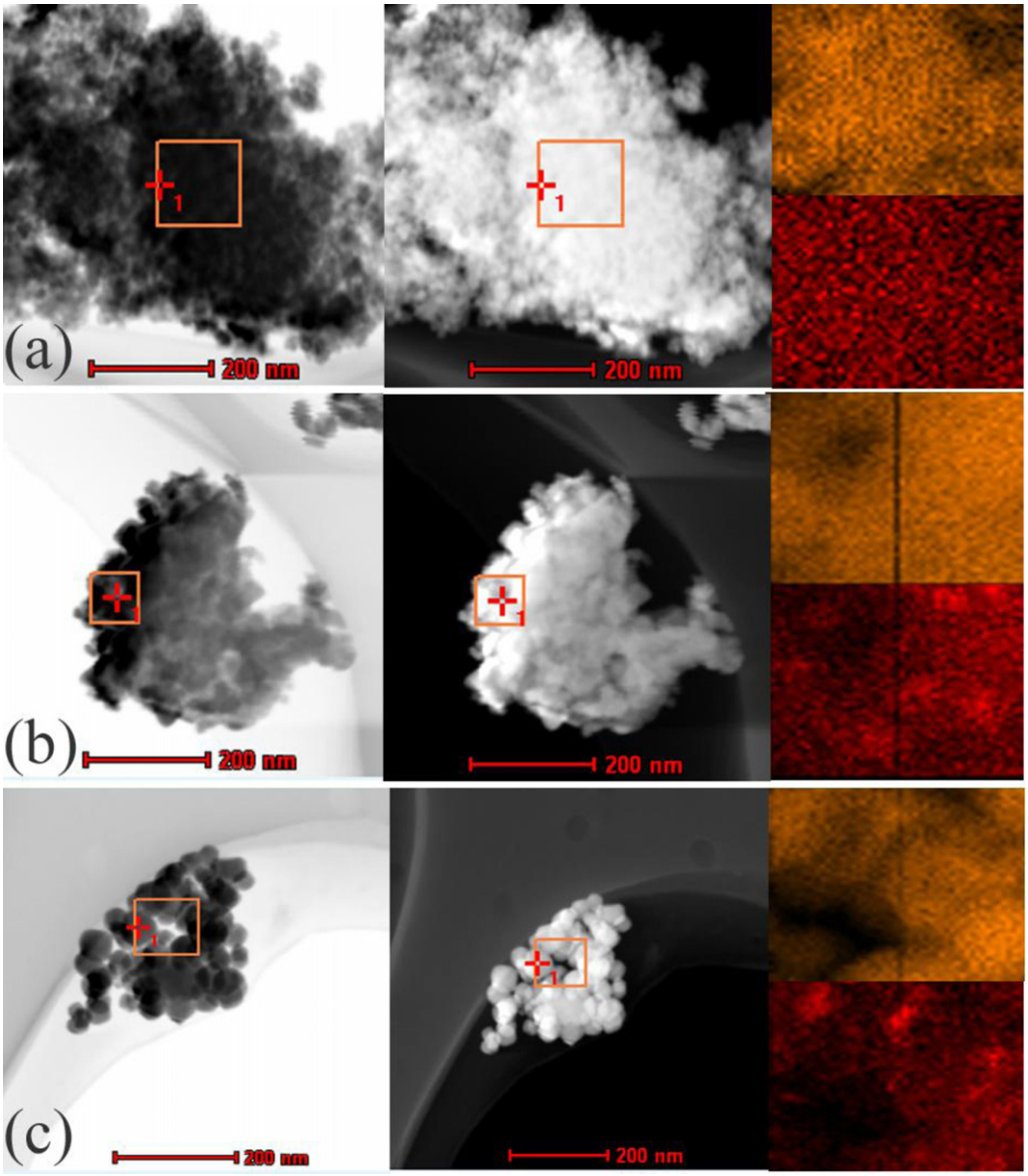

Fig. 3. STEM-EDS mapping images taken from a square region in (a) Pd/HY; (b) Pd/COM; (c) Pd/PI. (Orange stands for Ce while red stands for Pd).

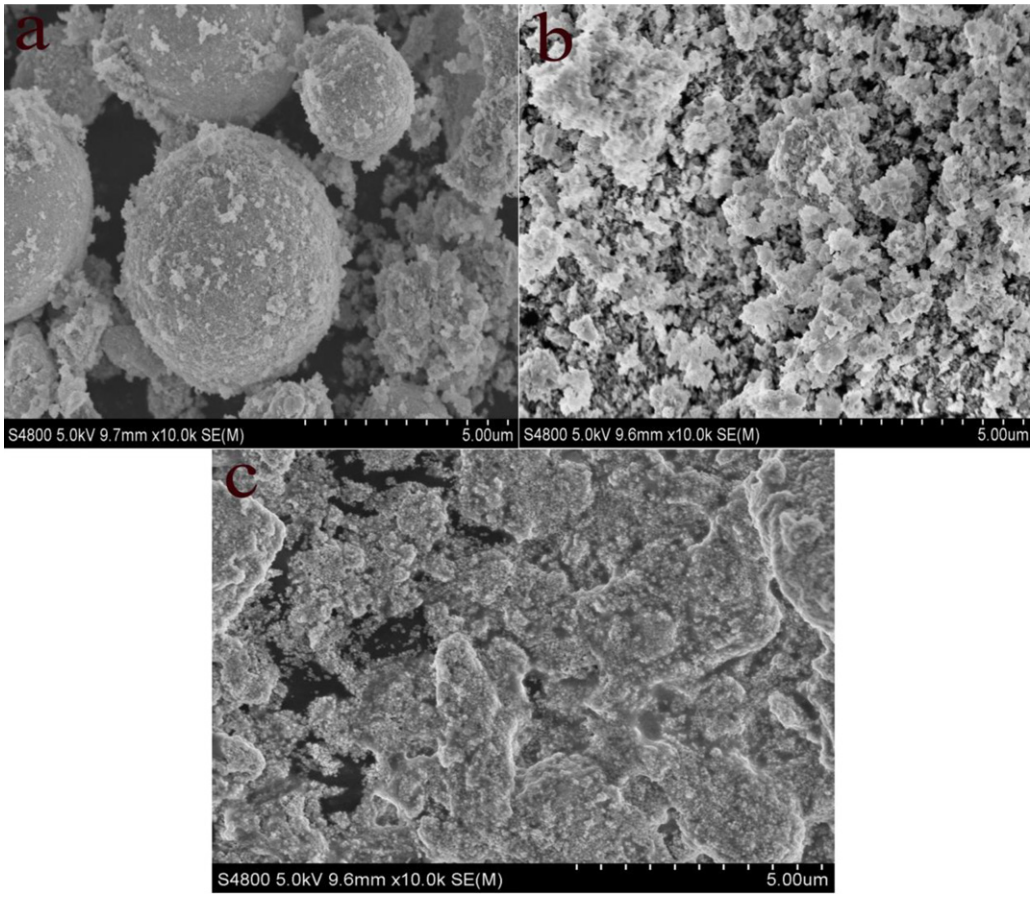

Fig. 4. SEM images of (a) Pd/HY; (b) Pd/COM; (c) Pd/PI.

catalytic active for certain reactions. Meanwhile, it appears that the lattice parameter of Pd/COM is the lowest, indicating the most incorporation of palladium ions into the CeO_2 lattice. This is because the ionic radius of Pd is smaller than that of Ce, leading to a decline in lattice parameter when a $Ce_{1-x}Pd_xO_{2-\delta}$ solid solution is formed. The phenomenon agrees with the fact that most palladium species exist in the form of ions when using a combustion method [18].

In order to quantify the content of surface palladium species, the Pd/HY, Pd/COM and Pd/PI catalysts were treated with HNO_3 by immersing them in 65 wt% HNO_3 (50 mL/g_{cat}) for 24 h. After that, the sample was filtrated and washed with distilled water sufficiently. The above process was repeated to ensure that surface palladium species can be completely removed. Finally the obtained sample was dried at 100 °C for 12 h, and the content of Pd in the catalyst was analyzed using atomic absorption spectrometry (AAS) after being dissolved by HCl and H_2O_2 mixed aqueous. The contents of total and surface Pd species are shown in Table 2, which seems to contradict with that the most palladium species incorporate into the CeO_2 lattice over the Pd/COM catalyst. It should be mentioned that not all of the bulk palladium species could be incorporated into the CeO_2 lattice. Nevertheless, it can be deduced that the more content of surface Pd, the less possibility of incorporation of Pd into the CeO_2 lattice. Hence, according to charge compensation, it is suggested that a lower concentration of oxygen vacancies will be obtained on Pd/PI since most palladium species exist on the surface of the catalyst.

Table 1 also lists the textural properties of catalysts. It is visible that the BET surface area of Pd/HY is larger than that of the other two catalysts. Meanwhile, the results of CO chemisorption listed in Table 2 show that Pd/HY has the highest Pd dispersion. Generally, the higher Pd dispersion and smaller Pd particle size produce higher active surface, resulting in a superior catalytic activity. And the higher Pd dispersion of the Pd/HY catalyst combined with its high BET area suggests good contact between the Pd and ceria phases, which is consistent with higher oxidation activity via a Mars-van Krevelen mechanism involving O-atom transfer from ceria to Pd. Additionally, in order to directly investigate the Pd distribution in the sample, the STEM-EDS mapping images are revealed in Fig. 3. It can be seen that Pd atoms are distributed uniformly over the entire observed area of Pd/HY. In contrast, Pd atoms are found either rich or lean in the regions of the other two catalysts, which is more apparent for Pd/PI. The finding also supports the results of CO chemisorption.

SEM images of catalysts are shown in Fig. 4. As displayed, different morphologies of catalysts are observed. The Pd/HY catalyst presents inhomogeneous 3D ball-like morphology while Pd/COM exhibits melting floc-like morphology as a lot of heat is released during combustion. Concerning Pd/PI, the particles aggregate together with irregular morphology, which might be related to its textural properties.

Fig. 5 depicts the XPS spectra of catalysts at Ce 3d core level. As illustrated in the figure, Ce 3d core spectra for all the samples were deconvoluted into eight peaks corresponding to four pairs of spin-orbit doublets. The four main $3d_{5/2}$ features at 881.6, 884.2, 887.8 and 897.5 eV are assigned to v, v', v'' and v''' components, while the $3d_{3/2}$ features at 900.1, 902.2, 906.8 and 916.1 eV are assigned to u, u', u'' and u''' components, respectively [22].

The signals v' and u' are typical for Ce^{3+} while the other signals are characteristic of Ce^{4+}. Meanwhile, the surface Ce^{3+} concentration of total Ce was semiquantitatively analyzed using the

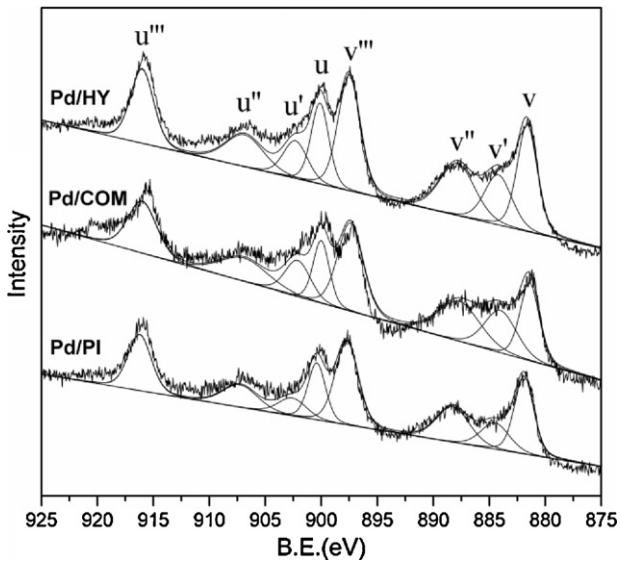

Fig. 5. Ce 3d XPS spectra of Pd/HY, Pd/COM and Pd/PI catalysts.

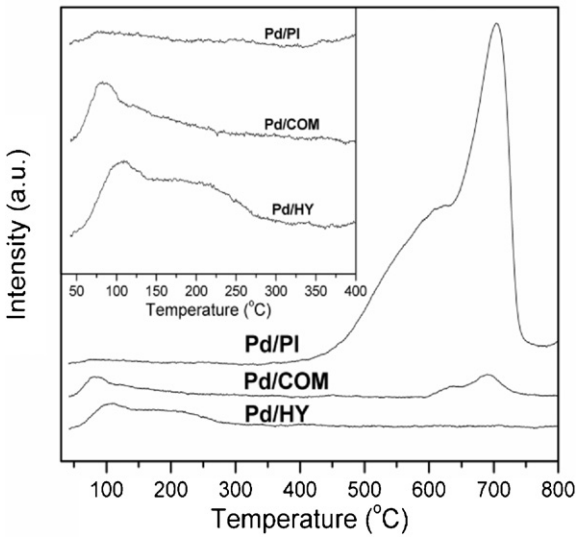

Fig. 7. O_2-TPD curves of Pd/HY, Pd/COM and Pd/PI catalysts.

integrated peak area of the respective valance states. As listed in Table 2, the values of Pd/HY, Pd/COM and Pd/PI are 17.2%, 20.0% and 14.1% respectively.

It has been reported in the literature that the higher Ce^{3+} concentration of total Ce that exists, the more oxygen vacancies form because oxygen vacancies can be produced via the transformation between Ce^{3+} and Ce^{4+} [23]. Hence, the Pd/COM catalyst possesses the most oxygen vacancies, one localized substitution defect [24], which will be helpful for the catalytic oxidation. On the other hand, most ionic palladium incorporates into the CeO_2 lattice in the case of Pd/COM, leading to a spontaneous formation of oxygen vacancies to maintain electroneutrality [25]. One issue may be put forward that why the Pd/HY catalyst with medium oxygen vacancies exhibits the best catalytic activity for co-oxidation of CO and methanol. It should be noted that defects include not only oxygen vacancies, and the comparison in defects of catalysts will be revealed in the following Raman analysis.

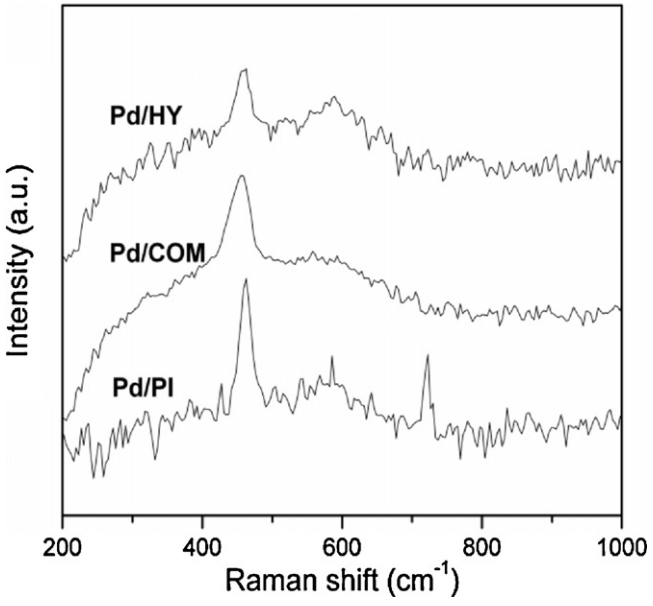

Fig. 6. Raman spectra of Pd/HY, Pd/COM and Pd/PI catalysts with 325 nm excitation laser line.

The UV (325 nm) Raman spectra, shown in Fig. 6, are applied to clarify the surface defects of the catalysts. The bands at 460 and 580 cm^{-1} belong to the F_{2g} symmetry mode [26] and defect-induced mode [27], respectively. For the Pd/PI catalyst, there is an additional band at 723 cm^{-1} ascribed to the vibration mode of Pd-O bond [28], implying a poor dispersion of PdO species on the catalyst surface. It is in line with the assessed dispersion. And the absence of Pd characteristic peaks in the XRD pattern of Pd/PI might be due to the combining effects of low loading and that diffraction lines of PdO ($2\theta = 27.3^\circ$, 31.7°, 45.5° PDF 46-1211) and PdO_2 ($2\theta = 28.0^\circ$, 35.3°, 54.5° PDF 34-1101) are very close to intensive diffraction lines of cubic CeO_2 phase.

The ratio between the intensities of 580 and 460 cm^{-1} Raman bands has been related to the degree of defect sites on CeO_2, and it is noted that the higher the I_{580}/I_{460} ratio, the higher the defects [29]. As seen in Table 2, the intensity ratio follows the sequence Pd/HY > Pd/COM > Pd/PI. It is therefore induced that the degree of defects is the highest over the Pd/HY catalyst, which is assumed for its least crystallinity and smallest crystallite size derived from XRD data. It is known that defects include not only oxygen vacancies but also step and edge defects, etc. Hence, high defects of a catalyst

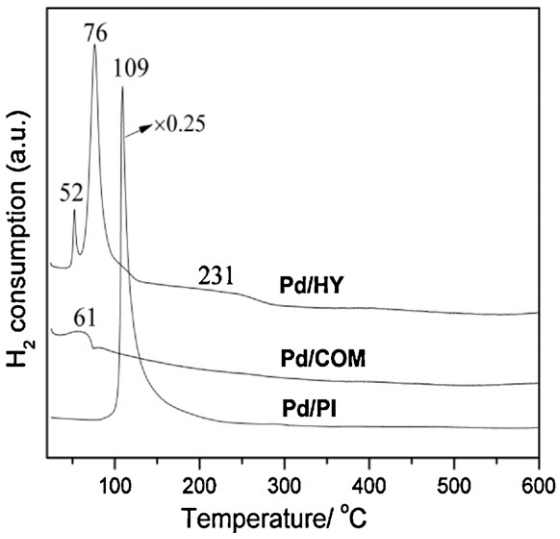

Fig. 8. H_2-TPR profiles of Pd/HY, Pd/COM and Pd/PI catalysts.

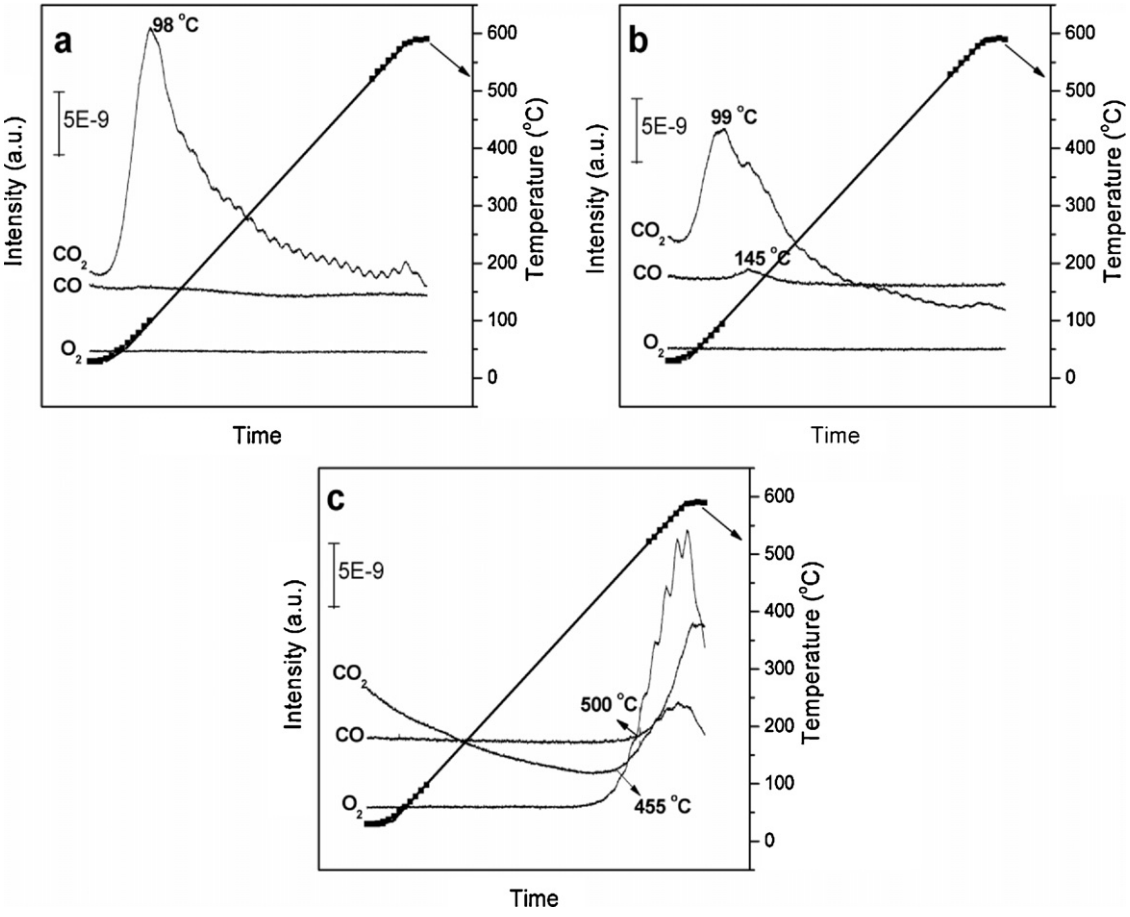

Fig. 9. Temperature programmed desorption profiles of CO over (a) Pd/HY; (b) Pd/COM; (c) Pd/PI.

do not correspond to large numbers of oxygen vacancies. A similar case was also found on Ni/CeO_2 nanostructures with different morphologies [30]. Whatever, the mobility of activated oxygen is high when more defect sites exist, which is crucial in the catalytic oxidation. It can be confirmed from that the sequence of I_{580}/I_{460} of catalysts is in accordance with their catalytic performances.

To further investigate the adsorption and activation of oxygen on the catalysts, O_2-TPD measurements were carried out, and the results are displayed in Fig. 7. As shown in Fig. 7, the desorption peak below 400 °C is ascribed to the surface active oxygen species while that above 500 °C should be assigned to the liberation of lattice oxygen [31]. And for supported Pd catalyst, the latter desorption peak corresponds to the decomposition of palladium oxide into metallic palladium [32].

Compared with Pd/HY, it is clear that the intensity of desorption peaks of surface active oxygen species on Pd/COM and Pd/PI decreases. In other words, more oxygen can be converted to active surface oxygen species over the Pd/HY catalyst. Then, the lattice oxygen of CeO_2 may be replenished in some way more quickly and thus the catalytic oxidation is promoted. Additionally, the desorption peaks at high temperature are only found on Pd/COM and Pd/PI catalysts. It was reported that stable PdO species are beneficial to the oxidation activity [33] and a higher temperature is requested for its desorption. And considering the fact that the charge state of surface Pd over Pd/HY is higher than that over Pd/COM deduced from Pd 3d XPS spectra (Fig. S1), we conclude that the Pd/HY catalyst possesses more stable PdO_x species. Taking into account both the abundant active surface oxygen species and stable PdO_x species, Pd/HY is expected to exhibit a better catalytic performance than the other two catalysts.

For metal oxide catalysts, H_2-TPR is a useful tool to obtain the reducibility of samples and the potential to remove or take up oxygen [34]. Therefore the lower reduction temperature is, the stronger is the redox ability of a catalyst. Since the co-oxidation of CO and methanol is expected to proceed at low temperatures, we especially focus on the low-temperature reduction properties of catalysts. The results of H_2-TPR of catalysts are presented in Fig. 8.

For the Pd/PI catalyst, one intensity peak at 109 °C is observed, which could be assigned to a reduction of surface PdO species [35]. And the amount of H_2 taken up is approximately 1901 μmol H_2/g, a quantity greater than 142 μmol H_2/g required to reduce Pd from PdO. Most of the additional H_2 uptake is due to the reduction of CeO_2 that is in contact with the Pd metal [36]. Regarding the Pd/COM catalyst, it can be noticed that the reduction peak shifts to a lower temperature, an indication of stronger redox ability. It is worth pointing out that the H_2 consumption of that peak is only 27 μmol H_2/g. It implies that these surface Pd species have a weak interaction with CeO_2 for an existing $Ce_{1-x}Pd_xO_{2-\delta}$ solid solution.

In the case of Pd/HY, three reduction peaks at 52, 76 and 231 °C are detected, and the corresponding H_2 consumptions are 18, 285 and 35 μmol H_2/g respectively. The former two peaks could be assigned to the reduction of surface PdO species and those bulk PdO species but not incorporating into the CeO_2 lattice, respectively. And the peak at high temperature above 100 °C may be associated with the reduction of surface oxygen [37]. As the first reduction peak consumes only 18 μmol H_2/g, this kind of PdO species contact weakly with CeO_2. Differently, another kind of PdO species characterized by a reduction peak at 76 °C interacts with the support to some extent for a consumption of 285 μmol H_2/g. Combining the fact that there is no reduction behavior of $Ce_{1-x}Pd_xO_{2-\delta}$ in

Pd/COM, we further confirm that some of bulk Palladium species in Pd/HY could combine with cerium to form Pd–Ce–O mixed oxide instead of $Ce_{1-x}Pd_xO_{2-\delta}$ solid solution. Moreover, the strong low-temperature redox ability is supposed to be caused by small crystallite size of CeO_2 [38] and average particle size of Pd. The above results indicate that the Pd/HY catalyst could give a better low-temperature catalytic performance in co-oxidation of CO and methanol.

As concluded before, the catalytic oxidation of CO is a rate-limited reaction for complete methanol oxidation at low temperature, therefore a TPD of CO is carried out and the results are illustrated in Fig. 9. It can be seen that all adsorbed CO desorbs as CO_2 for Pd/HY whereas there is also molecular desorption of CO for Pd/COM and Pd/PI. This indicates that the ability of catalytic CO oxidation is better on Pd/HY. Meanwhile, for Pd/HY and Pd/COM, the CO_2 profiles are characterized by a peak at ca. 98 °C, which is more intense for the former catalyst. And the onset temperature of producing CO_2 over Pd/PI is as high as 455 °C, implying a poor conversion of CO to CO_2 and thus an inhibition of methanol oxidation at low temperature. Additionally, a desorption of O_2 is observed over Pd/PI, corresponding to the decomposition of palladium oxide into metallic palladium. It is in agreement with the results of O_2-TPD.

4. Conclusions

CeO_2 supported Pd catalysts were prepared by three different methods and investigated in the co-oxidation of CO and methanol. It is shown that the Pd/HY catalyst exhibits a best performance, giving light-off temperatures of both CO and methanol conversions below 100 °C. And it is demonstrated that an easier catalytic oxidation of CO following the Mars-van Krevelen-type mechanism, an enhanced complete methanol oxidation. The reason is that the presence of CO will adsorb rapidly and strongly on the noble metal sites, inhibiting the complete methanol oxidation at low temperature. Hence, it is proposed that the outstanding catalytic activity of Pd/HY is mainly attributed to its high degree of defect sites, which can improve the mobility of activated oxygen and further enhance the reactivity of low-temperature CO oxidation and deep methanol oxidation. Interestingly, XPS analysis provides that Pd/COM possesses the largest oxygen vacancies, one contributor to defect sites. And the highest degree of total defect sites found on Pd/HY is speculated for the low crystallinity and small crystallite size of CeO_2 synthesized through a hydrothermal process. Meanwhile, high Pd dispersion and stable PdO_x species observed over Pd/HY are beneficial to the catalytic oxidation. Additionally, a superior redox ability found on Pd/HY correlates with its good low-temperature activity.

Acknowledgement

This work was financially supported by the Key Industrial Science-Technology Program of Fujian Province, China (2010H6014).

Appendix A. Supplementary data

Supplementary data associated with this article can be found, in the online version, at http://dx.doi.org/10.1016/j.apcatb.2013.02.020.

References

[1] J.J. Brey, I. Contreras, A.F. Carazo, R. Brey, A.G. Hernández-Díaz, A. Castro, Journal of Power Sources 169 (2007) 213–219.
[2] A.M. Pourkhesalian, A.H. Shamekhi, F. Salimi, Fuel 89 (2010) 1056–1063.
[3] X. Ou, X. Yan, X. Zhang, Z. Liu, Applied Energy 90 (2012) 218–224.
[4] T. Hu, Y. Wei, S. Liu, L. Zhou, Energy and Fuels 21 (2007) 171–175.
[5] Y. Wei, S. Liu, H. Li, R. Yang, J. Liu, Y. Wang, Energy and Fuels 22 (2008) 1254–1259.
[6] H. Zhao, Y. Ge, C. Hao, X. Han, M. Fu, L. Yu, A.N. Shah, Science of the Total Environment 408 (2010) 3607–3613.
[7] J. Vancoillie, J. Demuynck, L. Sileghem, M.V.D. Ginste, S. Verhelst, L. Brabant, L.V. Hoorebeke, Applied Energy 102 (2013) 140–149.
[8] R.W. McCabe, P.J. Mitchell, Applied Catalysis 27 (1986) 83–98.
[9] R.W. McCabe, P.J. Mitchell, Journal of Catalysis 103 (1987) 419–425.
[10] W. Wang, H. Zhang, G. Lin, Z. Xiong, Applied Catalysis B 24 (2000) 219–232.
[11] M.J. Lippits, R.R.H.B. Iwema, B.E. Nieuwenhuys, Catalysis Today 145 (2009) 27–33.
[12] Y. Luo, Y. Xiao, G. Cai, Y. Zheng, K. Wei, Catalysis Communications 27 (2012) 134–137.
[13] R.W. McCabe, P.J. Mitchell. Inventor, General Motors Corporation, assignee, United States Patent No. 4673,556; (1987 June 16).
[14] G. Cui, P.K. Shen, H. Meng, J. Zhao, G. Wu, Journal of Power Sources 196 (2011) 6125–6130.
[15] K. Liu, A. Wang, T. Zhang, ACS Catalysis 2 (2012) 1165–1178.
[16] A.I. Boronin, E.M. Slavinskaya, I.G. Danilova, R.V. Gulyaev, Y.I. Amosov, P.V. Kuznetsov, I.A. Polukhina, S.V. Koscheev, V.I. Zaikovskii, A.S. Noskov, Catalysis Today 144 (2009) 201–211.
[17] S. Hinokuma, H. Fujii, M. Okamoto, K. Ikeue, M. Machida, Chemistry of Materials 22 (2010) 6183–6190.
[18] M.S. Hegde, G. Madras, K.C. Patil, Accounts of Chemical Research 42 (2009) 704–712.
[19] T. Takeguchi, S. Manabe, R. Kikuchi, K. Eguchi, T. Kanazawa, S. Matsumoto, W. Ueda, Applied Catalysis A 293 (2005) 91–96.
[20] A. Trovarelli, Catalysis Reviews-Science and Engineering 38 (1996) 439–520.
[21] L. Meng, J. Lin, Z. Pu, L. Luo, A. Jia, W. Huang, M. Luo, J. Lu, Applied Catalysis B 119–120 (2012) 117–122.
[22] E. Bêche, P. Charvin, D. Perarnau, S. Abanades, G. Flamant, Surface and Interface Analysis 40 (2008) 264–267.
[23] X. Liu, K. Zhou, L. Wang, B. Wang, Y. Li, Journal of the American Chemical Society 131 (2009) 3140–3141.
[24] M. Yashima, H. Arashi, M. Kakihana, M. Yonshimura, Journal of the American Ceramic Society 77 (1994) 1067–1071.
[25] D.O. Scanlon, B.J. Morgan, G.W. Watson, Physical Chemistry Chemical Physics 12 (2011) 4279–4284.
[26] S. Deshpande, S. Paatil, S.V.N.T. Kuchibhatla, S. Seal, Applied Physics Letters 87 (2005) 133113.
[27] J.R. McBride, K.C. Hass, B.D. Poindexter, W.H. Weber, Journal of Applied Physics 76 (1994) 2435–2441.
[28] J.R. McBride, K.C. Hass, B.D. Poindexter, W.H. Weber, Physical Review B 44 (1991) 5016–5028.
[29] J. Lin, L. Li, Y. Huang, W. Zhang, X. Wang, A. Wang, T. Zhang, Journal of Physical Chemistry C 115 (2011) 16509.
[30] X. Du, D. Zhang, L. Shi, R. Gao, J. Zhang, Journal of Physical Chemistry C 116 (2012) 10009–10016.
[31] C. Ma, Z. Mu, J. Li, Y. Jin, J. Cheng, G. Lu, Z. Hao, S. Qiao, Journal of the American Chemical Society 132 (2010) 2608–2613.
[32] M. Luo, X. Zheng, Applied Catalysis A 189 (1999) 15–21.
[33] R. Zhou, B. Zhao, B. Yue, Applied Surface Science 254 (2008) 4701–4707.
[34] Z. Zhao, Y. Yamada, A. Ueda, H. Sakurai, T. Kobayashi, Catalysis Today 93–95 (2004) 163–171.
[35] L. Ma, M. Luo, L. Han, S. Chen, Catalysis Letters 70 (2000) 357–362.
[36] H. Zhu, Z. Qin, W. Shan, W. Shen, J. Wang, Journal of Catalysis 225 (2004) 267–277.
[37] Q. Wang, G. Li, B. Zhao, M. Shen, R. Zhou, Applied Catalysis B 101 (2010) 150–159.
[38] M. Kurnatowska, L. Kepinski, W. Mista, Applied Catalysis B 117-118 (2012) 135–147.